Indian Journal of Pure & Applied Physics
Vol. 53, February 2015, pp. 119-124

Effect of Ni doping on ferroelectric, dielectric and magneto dielectric properties of strontium barium niobate ceramics

S H Kshirsagar[a], A N Tarale[a], S R Jigajeni[b*], D J Salunkhe[a] & P B Joshi[a]

[a]Solapur University, Solapur (M S), 413 255, India

[b]Walchand Institute of Technology, Solapur (M S), India

E-mail: suvarnahkshirsagar@yahoo.com

Received 2 July 2014; revised 11 August 2014; accepted 23 December 2014

To understand possible interactions between magnetic and electric order parameters of Ni doped $Sr_xBa_{1-x}Nb_2O_6$, Ni doped $Sr_{0.5}Ba_{0.5}Nb_2O_6$ (SBN50) and $Sr_{0.4}$ $Ba_{0.6}$ Nb_2 O_6 (SBN40) are synthesized and investigated. Synthesis has been carried out via ceramic route. The paper reports the synthesis, crystal structure, dielectric properties, PE hysteresis loops, M-H hysteresis loops and magneto-capacitance of the Ni doped SBN compositions. All the compositions are observed to exhibit a useful value of magneto-capacitance, especially at frequencies less than 10 kHz.

Keywords: $Sr_{0.4}$ $Ba_{0.6}$ Nb_2 O_6 (SBN40), Ni doped SBN, Relaxor, PE Hysteresis, Magneto-dielectric

1 Introduction

$Sr_xBa_{1-x}Nb_2O_6$ (SBN) is known to be a relaxor ferroelectric exhibiting tetragonal tungsten bronze (TTB) crystal structure[1,2]. To enhance the dielectric and ferroelectric properties doping effects have been studied. Essentially, transition metal/rare earth doped single crystal and polycrystalline SBN systems are widely investigated, owing to their applications in the field of piezoelectric, pyroelectric, electro-optic, non-linear optic, holographic recording devices[3-8].

Tetragonal strontium-barium-niobate undergoes a relaxor type phase transition from a ferro to a paraelectric phase, with no strong structural changes, besides losing its center of inversion. Ferro electricity in SBN is believed to occur due to dynamics and properties of nano domains[9] (polar clusters). Therefore, the transition temperature (T_m) and its diffuseness for SBN are critically dependent on the (Sr)/(Ba) ratio. The value of T_m also depends on doping of the SBN by the transition metal elements or rare earth elements[9,10]. Additionally, it is observed that the transition temperature of SBN also depends on particle size and its distribution[11,12]. It is observed that the temperature of dielectric maximum (T_m) i.e. transition temperature decreases with increase in the level of substitution. Further, it is also observed that P-E hysteresis persists for temperatures well above the transition temperature and the substitution of transition metals like Ni causes reduction in the coercive field and improves switching properties[4,13] of SBN.

Amongst the doped SBN compositions, Cr, Mn, Fe, Co and Ni doped SBN systems may form a special class of doped systems. These compositions may possess interactions between magnetic and electric order parameters. Further, it is known that the Ni exhibits various oxidation states in addition to their most common oxidation states, viz. +2 and +3. Therefore, it is possible to synthesize Ni doped SBN systems without much increase in the value of loss tangent (tan δ). It is already reported that the Fe doped $PbTiO_3$ and Pb (Sr) TiO_3 show the presence of both ferroelectric and ferromagnetic orders at room temperature[14,15]. In addition to the substitution of Fe, substitution of Co or Ni may cause a coupling between electric and magnetic order parameters.

Hence, it is proposed to investigate Ni doped SBN systems, such that the ferroelectric transition temperature of the resulting systems occur in the vicinity of room temperature. A possible virtue of these compositions would be a remarkable magneto dielectric coupling, measured in terms of the magneto-capacitance (M_c). The magneto-capacitance M_c defined as $M_c=[\varepsilon(H) - \varepsilon(0)]/\varepsilon(0)$, where $\varepsilon(H)$ and $\varepsilon(0)$ are the dielectric constants in the presence and absence of the applied magnetic field [16]. Therefore, the present paper reports synthesis, crystal structure, dielectric properties, P-E hysteresis loops, M-H hysteresis loops and magneto dielectric properties of the following systems.

$Sr_{0.5}Ba_{0.5}Nb_{2-x}Ni_xO_6$ for (x=0.0, 0.02, 0.03) and $Sr_{0.4}Ba_{0.6}Nb_{2-x}Ni_xO_6$ for (x=0.0, 0.05, 0.10)

The compositions of $Sr_{0.5}Ba_{0.5}Nb_{2-x}$ Ni_xO_6 for (x = 0.0, 0.02, 0.03) are abbreviated as SBN50, SBNNi02, SBNNi03, respectively. Further, the compositions of $Sr_{0.4}Ba_{0.6}Nb_{2-x}Ni_xO_6$ for (x = 0.0, 0.05 and 0.10) are abbreviated as SBN40, SBNNi05, SBNNi10, respectively.

2 Experimental Details

The precursors used for synthesis of pure and Ni doped SBN via ceramic route of synthesis were AR grade $BaCO_3$, $SrCO_3$, Nb_2O_5 and NiO. Stoichiometric amounts of starting chemicals were mixed thoroughly in an agate mortar-pestle for 2 h. Calcination was carried out at 1150°C for 12 h, while final sintering was carried out at 1250°C for 24 h, with an intermediate process of grinding. After the process of intermediate grinding, the powder was pressed in the form of disc shaped samples. These samples were used for measurements of the crystal structure, dielectric properties, magneto dielectric properties and P-E hysteresis loops. The M-H hysteresis loops were determined on the powdered samples.

X-ray diffractograms were determined using 'Brucker axs' (D8 advance) X-ray diffractometer. The dielectric constant was measured as a function of frequency, temperature and magnetic field, using HP4284 LCR-Q meter, a custom built furnace set up and an electromagnet from Scientific Equipment and services, Roorkee (EMU-75). The P-E hysteresis loops were determined using P-E hysteresis loop tracer due to M/S Marine India Limited, New Delhi. M-H hysteresis loops were determined using Vibrating Sample Magnetometer (VSM) due to Lakeshore model No.7307.

3 Results and Discussion

3.1 Structural Properties

Figure 1(a, b and c) shows X-ray diffractograms of SBN50, SBNNi02 and SBNNi03, respectively. Further, Fig. 2(a, b and c) shows the X-ray diffractograms of SBN40, SBNNi05 and SBNNi10, respectively. It is seen from Figs 1 and 2 that all the peaks in the X-ray diffractograms could be indexed using JCPDs data of SBN50 (Card No.39-0265). Further no impurity peaks are seen in the X-ray diffractograms of Figs 1 and 2. Therefore, it appears that all the compositions studied are synthesized in the tetragonal tungsten bronze (TTB) crystal structure and corresponding lattice parameters are presented in Table 1. The crystallite size is determined by using Scherrer's formula and is also presented in Table 1. From Table 1, it is observed that the lattice parameters a and c determined in the present case are found to be in good agreement with the earlier reports[17]. Further, it is also observed that lattice parameters a and c decrease with increasing level of

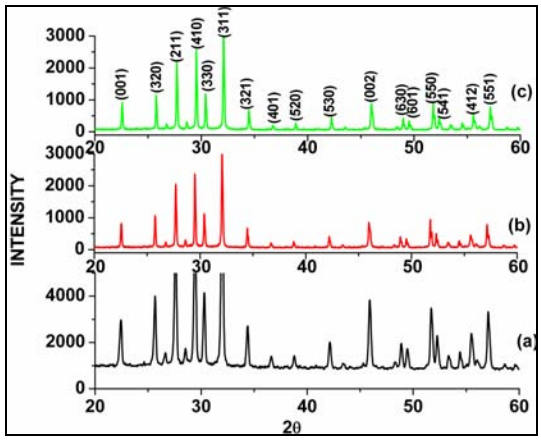

Fig. 1 — X ray diffractogram of (a) SBN50 (b) SBNNi02 (C) SBNNi03

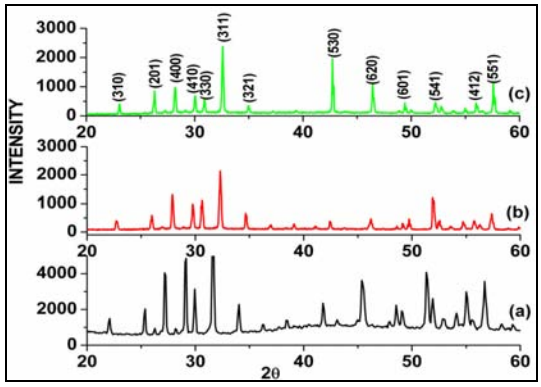

Fig. 2 — X ray diffractogram of (a) SBN40 (b) SBNNi05 (C) SBNNi10

Table1 — Lattice parameters of SBN50, SBN40 and Ni doped SBN compositions with their crystallite size

Composite	a Å	c Å	c/a	Crystallite size nm
SBN50	12.483	3.951	0.317	68
SBNNi02	12.469	3.946	0.316	103
SBNNi03	12.457	3.943	0.317	103
SBN40	12.641	3.991	0.316	75
SBNNi05	12.362	3.933	0.318	78
SBNNi10	12.239	3.908	0.319	92

substitution of Ni. It is known that substitution of Ni causes creation of certain oxygen vacancies and compaction of unit cell. This phenomenon may lead to the reduction of the lattice parameters.

3.2 Dielectric Properties

Figure 3(a and b) shows the variation of dielectric constant (ε) as a function of temperature at frequencies 1, 10, 100 kHz and 1 MHz for SBN50 and SBN40, respectively. Here ε is determined as a relative value, with respect to the dielectric constant of free space, ε_0. It is seen from Fig. 3(a and b) that the dielectric constant passes through a peak at temperature T_m (Temperature at maximum value of dielectric constant) for SBN50 and SBN40. T_m at 10 kHz for SBN50 is in good agreement with the previous reports on SBN system synthesized via ceramic route of synthesis [12]. Here, T_m is observed to increase with increase in frequency. The variation of ε for ($T > T_m$) has been fitted to an equation:

$$\frac{1}{\varepsilon} = \frac{1}{\varepsilon_{\max}} + \frac{(T - T_m)^{\gamma}}{2\varepsilon_{\max}\delta^2} \qquad \ldots(1)$$

where ε is the dielectric constant, ε_{max} the maximum value of the dielectric constant at temperature T_m, γ the diffuseness constant and δ is a diffusivity parameter [18].

Figure 4(a and b) shows the variation of $\log(1/\varepsilon - 1/\varepsilon_{\max})$ versus $\log(T - T_m)$, variation of ε at frequencies 10 kHz, 100 kHz, 1 MHz for SBN50 and SBN40, respectively. From Fig. 4(a and b), it is observed that $\log(1/\varepsilon - 1/\varepsilon_{\max})$ versus $\log(T - T_m)$ shows a linear behaviour for temperatures between 8 to 20 K above T_m. However, for lower frequencies i.e. 1 kHz a small non-linearity is seen for temperatures up to 10 K above T_m. This observation suggests that the SBN50 as well as SBN40 shows the behaviour similar to a relaxor ferroelectric[13]. The curve fitting parameters γ and δ are determined for all the frequencies of the measurements and are presented in Tables 2 and 3 for SBN50 and SBN40, respectively. Tables 2 and 3 also presents the variation of ε at room temperature (ε_{RT}), tan δ at room temperature (tan δ_{RT}), ε_{max} and T_m, as a function of varying frequency for SBN50 and SBN40, respectively. From Tables 2 and 3, it is observed that the value of γ is between 1 and 2. For conventional ferroelectric materials, it is known that the exponent γ of Eq. (1) is equal to 1, while for the ferroelectric materials with completely diffused phase transition the value of γ is nearly equal to 2.

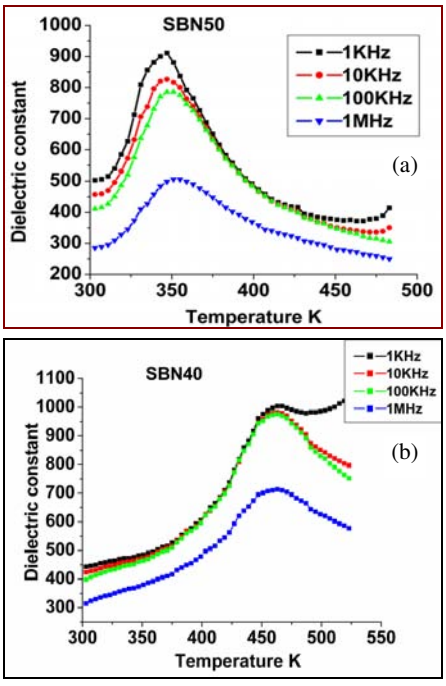

Fig. 3 — Variation of dielectric constant (ε) with temperature at frequencies 1 kHz 10 kHz, 100 kHz and 1 MHz for (a) SBN50 and (b) SBN40 composition

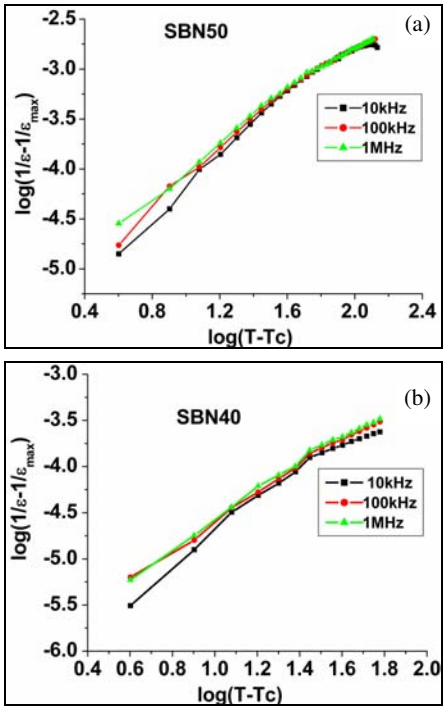

Fig. 4 — Variation of $\log(1/\varepsilon - 1/\varepsilon_{max})$ versus log ($T\text{-}T_m$), variation of ε at frequencies 10 kHz, 100 kHz, 1 MHz for (a) SBN50 and (b) SBN40

These materials are termed as relaxors. For γ between 1 and 2, the phase transition is partially diffused and the corresponding materials are termed as partial relaxors[18]. Therefore, essentially SBN50 and SBN40 show a partial relaxor behaviour.

Figure 5(a and b) shows the variation of ε as a function of temperature T at frequencies 1, 10, 100 kHz and 1 MHz for SBNNi03 and SBNNi10, respectively. Further, the variation of ε with T for SBN Ni02 and SBNNi05, is similar in nature to the variations shown in Fig. 5(a and b). It could be seen that the variation of ε versus T for Ni doped SBN is similar in nature to the SBN50 and SBN40. Therefore, the variation of ε versus T for all the Ni doped samples are fitted to Eq. (1). Table 4 presents the variation of, ε_{RT}, tan δ_{RT}, ε_{max}, T_m, γ, and δ for all the Ni doped samples at f =10 kHz. From Table 4, it is seen that the value of γ is always between 1 and 2. However, T_m for Ni doped SBN is observed independent of the frequency of the measurement. Therefore, it appears that the substitution of Ni suppresses the relaxor behaviour of SBN50 and SBN40. Nevertheless, as γ is greater than 1, the nature of transition is still a non Curie-Weiss type. Such a transition is termed as diffused phase transition (DPT). From Table 4, it is seen that T_m decreases as the level of substitution increases. However, the values of ε_{RT} and ε_{max} decrease as the Ni concentration increases. Similar observations are reported for Fe doped SBN50, where it is reported that ε initially increases with increase in substitution of Fe and then decreases as Fe concentration is increased further[13]. Further, it is interesting to note that the tanδ for the Ni doped systems is of the same order of magnitude as that of parent SBN compositions. Ni, is known to be a '*d*' shell material with primary oxidation state +2. Therefore, the doping of Ni is non-isoelectric. The non-isoelectric doping may lead to localized oxygen vacancies. At present, the percentage of oxygen vacancies is not determined quantitatively as level of the doping is very low. However, it appears that despite of the presence of oxygen vacancies the loss in the doped compositions remains unchanged.

Table 2 — Values of ε_{RT}, tanδ_{RT}, ε_{max}, T_m, γ and δ for SBN50 at all frequencies

Frequency (Hz)	ε_{RT}	tanδ_{RT}	ε_{max}	T_m	γ	δ
1000	503.420	0.065	917.884	347	1.153	7.42E-05
10000	457.637	0.071	826.524	347	1.510	3.79E-05
100000	411.295	0.086	785.812	351	1.372	5.05E-05
1000000	286.196	0.206	506.414	355	1.430	6.18E-05

Table 3 — Values of ε_{RT}, tanδ_{RT}, ε_{max}, T_m, γ and δ for SBN40 at all frequencies

Frequency (Hz)	ε_{RT}	tanδ_{RT}	ε_{max}	T_m	γ	δ
1000	443.538	0.031	1003.955	463	1.375	1.41E-05
10000	424.058	0.033	982.977	463	1.360	2.4E-05
100000	398.585	0.052	976.983	463	1.339	2.6E-05
1000000	314.672	0.140	713.257	463	1.350	3.21E-05

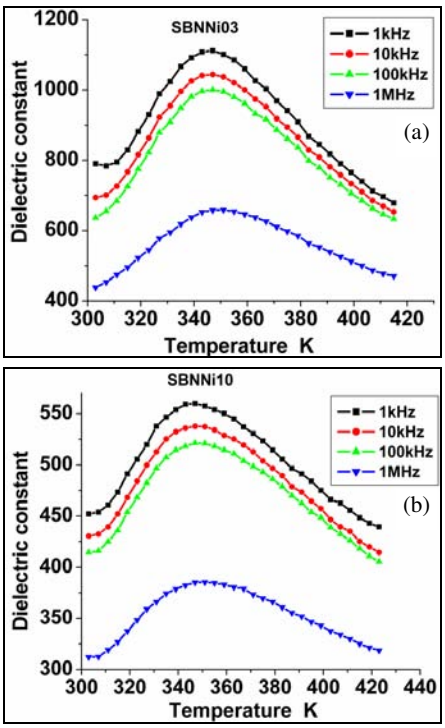

Fig. 5 — Variation of dielectric constant (ε) with temperature at frequencies 1 kHz, 10 kHz, 100 kHz and 1 MHz for (a) SBNNi03 and (b) SBNNi10 composition

3.3 P-E Hysteresis loop

Figure 6(a) shows the P-E hysteresis loops for SBN50, SBNNi02 and SBNNi03; while Fig. 6 (b) shows P-E hysteresis loops for SBN40, SBNNi05 and SBNNi10. From Fig. 6(a), it is seen that the magnitude of maximum value of polarization P_{max}

Table 4 — Values of ε_{RT}, tanδ_{RT}, ε_{max}, T_m, γ and δ for f = 10 kHz for Ni doped SBN compositions

Composite	ε_{RT}	tanδ_{RT}	ε_{max}	T_m	γ	δ
SBNNi02	1193.973	0.027	2638.686	359	1.629	1.267E-05
SBNNi03	693.940	0.077	1043.879	347	1.301	2.767E-05
SBNNi05	368.780	0.044	635.556	383	1.371	3.563E-05
SBNNi10	430.563	0.031	537.757	347	1.643	2.015E-05

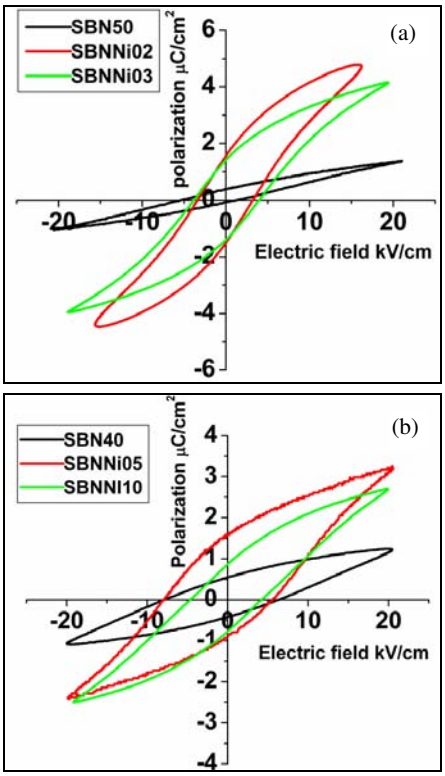

Fig. 6 — P-E hysteresis loop for (a) SBN50, SBNNi02 and SBNNi03 and (b) SBN40, SBNNi05 and SBNNi10

Table 5 — Maximum polarization $P_{max,}$ remnant polarization P_r and coercive field E_c for SBN50, SBN40 and Ni doped SBN compositions

Composition	P_{max}	P_r	E_c	P_r/P_{max}
SBN50	1.23	0.23	3.36	0.19
SBNNi02	4.66	1.55	3.26	0.33
SBNNi03	4.11	1.42	3.92	0.35
SBN40	1.17	0.48	7.00	0.41
SBNNi05	2.83	1.24	6.68	0.44
SBNNi10	2.62	0.83	4.57	0.32

increases initially for substitution of Ni at 2% but then decreases slightly as the level of substitution becomes 3%. Similar are the observations for SBNNi05 and SBNNi10. A similar trend is also seen in the variation in the dielectric constant of Ni doped SBN50 and SBN40 (Table 5). Initial increase in ε and P_{max} may partially correspond to the decrease in cell volume of the Ni doped SBN compositions. However, the polarization due to off centered Ni or Nb ions may occur in random directions[13]. These random orientations of local polar domains may lead to a reduction in the polarization per unit cell, as the Ni

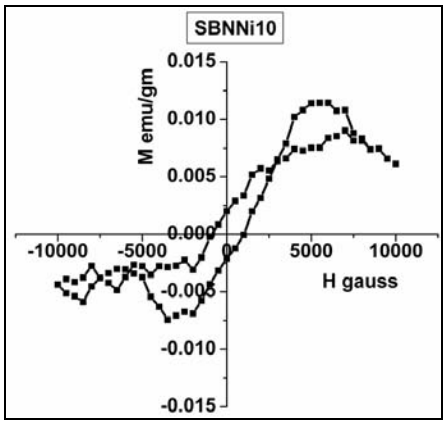

Fig. 7 — M-H hysteresis loop for SBNNi10

concentration increases beyond a certain concentration. Further, the remnant polarization P_r and coercive field E_c are observed to decrease as the concentration of Ni increases from 2% to 3% or 5% to 10%. These observations are similar to the earlier reports on the Fe, Ni, Cr doped[4,5,13] SBN.

3.4 M-H Hysteresis loop

To understand possible magnetic ordering in Ni doped SBN, M-H hysteresis loop for SBNNi10 is determined. Here, the percentage of Ni ions is the maximum amongst the compositions being investigated in the present case. Fig. 7 shows M-H hysteresis loop for SBNNi10. The composition appears to be a weak ferromagnet, near its curie temperature (Fig. 7). In the present case, the level of substitution of Ni ion is very low, i.e. 1 atom per 10 unit cells for SBNNi10. Therefore, we may not expect any direct or indirect long range exchange field to exist. Therefore, the magnetic moment per Ni atom is very low as compared to the magnetic moments of Ni^{2+} and Ni^{3+} ions. Similar observations[14] are reported for $(Pb_{1-x}Sr_x)$ $Ti_{0.988}Fe_{0.012}O_3$. Consequently, it is expected that the electromagnetic induction in the present case may exist only in certain local regions of Nb-O-Ni-O-Nb chains.

3.5 Magneto-dielectric properties

Fig. 8(a and b) shows the variation of dielectric constant versus frequency at applied magnetic field H = 0.0 T and H = 0.6 T, for SBNNi03 and SBNNi10, respectively. It could be seen from Fig. 8(a and b) that both the compositions possess a useful amount of magneto-dielectric coupling. Similar are the observations for the remaining Ni doped SBN compositions. Table 6 presents the magnitudes of M_c

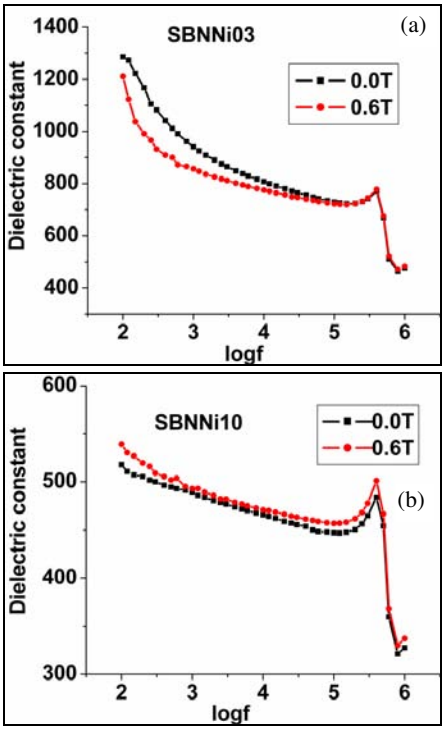

Fig. 8 — Variation of dielectric constant (ε) with frequency (log$F$) for applied magnetic field H = 0.0T and 0.6 T, for (a) SBNNi03 and (b) SBNNi10

Table 6 — Variation of magneto-capacitance (M_c) with Ni doped SBN compositions for frequencies 100 Hz, 500 Hz, 1 kHz, 10 kHz, 100 kHz, and 500 kHz

Frequency (Hz)	Compositions			
	SBNNi02 M_c (%)	SBNNi03 M_c (%)	SBNNi05 M_c (%)	SBNNi10 M_c (%)
100	15.10	-5.86	5.36	4.14
500	4.37	-11.06	3.01	1.44
1000	4.59	-8.98	2.15	0.73
10000	4.42	-4.02	3.10	1.11
100000	5.19	-0.96	3.48	2.21
500000	4.12	1.22	3.53	2.73

at 100 Hz, 500 Hz, 1 kHz, 10 kHz, 100 kHz, and 500 kHz for all the compositions studied in the present case. It could be seen that the relative magnitudes of M_c are higher at lower frequencies. Further, the magnitudes are also higher for SBNNi03 and SBNNi10, where T_m is slightly above room temperature.

4 Conclusions

The Ni doped SBN compositions could be synthesized via ceramic route of synthesis. The observations on crystal structure show that the Ni doped SBN systems exhibit the TTB crystal structure. The lattice parameters decreased slightly with increase in level of substitution. The substitution of Ni causes reduction in the Curie temperature with increase in level of substitution. The observations on ferroelectric hysteresis loops are consistent with the observed dielectric property. All the compositions are observed to exhibit a characteristic magneto-dielectric coupling with a useful value of magneto-capacitance M_c.

Acknowledgement

The authors wish to acknowledge a help rendered by Dr. Y. D. Kolekar, Department of Physics, University of Pune, Maharashtra, India, for the measurements of P-E and M-H hysteresis loops.

References

1 Neurgaonkar R R, Oliver J R, Cory W K, Cross L E & Viehland D, *Ferroelectrics*, 160 (1994) 265.
2 Mendes R G, Araújo E B & Eiras J A, *Materials Res*, 4(2) (2001) 113.
3 Kaczmarek S M, Orlowski M, Skibinski T, Jasik A & Ivleva L I, *Rev Adv Mater Sci*, (2010) 80.
4 Matyjasek K, Wolska K, Kaczmarek S M, Subocz J & Ivleva L, *Appl Phys B*, 106 (2012) 143.
5 Volk T, Isakov D, Salobutin V, Ivleva L, Lykov P, Ramzaev V & Wo¨hleckec M, *Solid State Communi,* 130 (2004) 223.
6 Glass A M, *J Appl Phys*, 40 (1969) 4699.
7 Liu S T, Maciolek R B, Zook J D & Rajagopalan B, *Ferroelectrics,* 87 (1988) 265.
8 Xu Y, Chen H C & Liu S T, *Jpn J Appl Phys*, 24 (1985) 278.
9 Volk T, Ivleva L, Lykov P, Pollok N, Salobutin V, Pankrath R & Wohlecke M, *Optical Materials*, 18 (2001) 179.
10 David C, Granzow T, Tunyagi A, W¨ohlecke M, Woike Th, Betzler K, Ulex M, Imlau M & Pankrath R, *Phys Stat sol*, (a) 201:R49-R52 (2004).
11 Patro P K, Kulkarni A R, Gupta S M & Harendranath C S, *Defence Sci J*, 57(1) (2007), 79.
12 Patro P K, International Symposium of Research Students on Materials Science and Engineering, December 20-22, (2004) Chennai, India.
13 Kim J S, Cho S Y & Jang M S, *J of the Korean Physic Society,* 51(2) (2007) 692.
14 Verma K C, Ram M, Kotnala R K, Bhatt S S & Negi N S, *Indian J of Pure & Appl Phys*, 48 (2010) 593.
15 Palkar V R, Purandare S C, Gohil S, John J & Bhattacharya S, *Appl Phys Lett*, 90 (2007) 172901.
16 Sutar M M, Tarale A N, Jigajeni S R, Kulkarni S B, Reddy V R & Joshi P B, *Solid State Sci*, 14 (2012) 1064.
17 Podlozhenov S, Graetsch H A, Schneider J, Ulex M, W¨ohlecke M & Betzler K, *Acta Crystallographica Section B*, B62 (2006) 960.
18 Niemer A, Pankrath R, Betzler K, Burianek M & Muehlberg M, *World J of Condensed Matter Phys*, 2 (2012) 80.